Enkephalin-mediated modulation of basal somatic sensitivity by regulatory T cells in mice

Nicolas Aubert [1], Madeleine Purcarea [1], Marie Fornier [1], Léonie Cagnet [1] , Marie Naturel [1], Armanda Casrouge [1], Gilles Dietrich [2], Marie-Caroline Dieu-Nosjean [1], Gilles Marodon [1,*]

1 UMRS 1135 Sorbonne Université, Inserm U1135, Centre d'Immunologie et des Maladies Infectieuses (CIMI-PARIS), 75013 Paris, France

2 IRSD, Université de Toulouse, INSERM, INRAE, ENVT, Univ Toulouse III - Paul Sabatier (UPS), Toulouse, France

* corresponding author : gilles.marodon@inserm.fr

Abstract

$CD4^+CD25^+Foxp3^+$ regulatory T cells (Treg) have been implicated in pain modulation in various inflammatory conditions. However, the mechanisms by which Treg hamper pain are still unclear. From a meta-analysis of 11 available transcriptomes, we show that the proenkephalin gene (*Penk)* which encodes the precursor of analgesic opioid peptides, is among the top 10 genes enriched in murine Treg relative to conventional T cells (Tconv). We then show that *Penk* expression in Treg is under the control of TNFR signaling and the transcription factor BATF. Using mice in which *Penk* mRNA expression can be tracked with a fluorescent reporter, we also show that *Penk* expression is restricted to Treg and activated Tconv in non-inflammatory conditions in all examined organs and tissues. Furthermore, inducible ablation of *Penk* in Treg leads to heat hyperalgesia for both male and female mice. Overall, our results indicate that TNFR signaling and BATF regulation of *Penk* in Treg might play a key role at modulating basal somatic sensitivity in mice.

Introduction

Regulatory T-cells (Treg), characterized by the expression of the alpha chain of the interleukin-2 receptor CD25 and the transcription factor Foxp3 [1], are known to be key players in immuno-regulation in both humans and mice; too few may lead to autoimmune diseases whereas too many may prevent an efficient immune response to cancer[2,3]. Over the last few years, several new functions of Treg beyond immunoregulation have been identified in tissue regeneration or local regulation of metabolism[4–6] for instance. In addition, there are accumulating evidences of a cross-talk between Treg and the nervous system. These includes promotion of oligodendrocyte differentiation or inhibition of neuroinflammation facilitating CNS repair process after brain injuries and preventing cognitive decline[7–10]. Furthermore, Treg have been involved in the regulation of pain in various model of nerve injury in rats and mice, such as in autoimmune neuritis or chronic constriction of the sciatic nerve[11–13]. Depletion of Treg have been associated with enhanced pain sensitivity whereas increased Treg number or activity limit pain hypersensitivity[14]. Although the current view is that Treg control pain through their immuno-suppressive functions [15], whether Treg might regulate pain at steady state is currently unknown. Starting from our previous observation that the expression of the proenkephalin gene (*Penk*), encoding for analgesic enkephalins, is highly enriched in Treg (Aubert et al., 2019 biorXiv, https://doi.org/10.1101/638072), we characterize the expression of *Penk* in the immune system and investigate the role of Treg on pain *in vivo* at steady state using advanced genetically-engineered mouse models. Our results uncover a previously unknown mechanism by which Treg modulate basal somatic sensitivity.

Results and Discussion

51 **A meta-signature of murine Treg and *Penk* expression in lymphoid and non-lymphoid**
52 **organs**

53 Using 11 available transcriptomes retrieved from the GEO website, we generated a Treg
54 molecular signature at steady state in lymphoid tissues, improving the robustness of the
55 analysis by several orders of magnitude relative to individual studies. The 25 most
56 differentially expressed genes are depicted in Figure 1A and the complete list is shown in
57 Table S1. As expected from the sorting strategies used to isolate Treg (Table 1 in the Material
58 and Methods section), we observe that *Il2ra* and *Foxp3* are the most differentially expressed
59 genes in Treg compared to Tconv, followed by the well-known Treg markers *CTLA-4, Itgae*
60 (CD103), *Ikzf2* (Helios) and *Klrg1*. However, several unexpected genes are present in that
61 signature, including the proenkephalin gene *Penk*, coding for opioid peptides endowed with
62 analgesic properties. Using the Immuno-Navigator database[16], a batch-corrected collection of
63 RNA quantification across numerous studies, samples and cell types, we confirm that *Penk* is
64 highly correlated to *Foxp3* in mice (R=0.871, Figure 1B). Enriched expression of *Penk* in Treg
65 was previously reported in several specific contexts including TCR-transgenic mice[17], UVB-
66 exposure[6] or in the brain of mice recovering from stroke[8]. Using publicly available datasets,
67 we also observe that *Penk* is enriched in Treg in the thymus, the visceral adipose tissue and in
68 muscles (Figure 1C). Thus, *Penk* mRNA expression in Treg is consubstantial of their generation
69 and is independent of their tissue localization at steady state.

70 ***Penk* mRNA expression is regulated by TNFR signaling and the BATF transcription factor in**
71 **Treg**

72 To explore possible mechanisms that could explain the enrichment of Penk mRNA in Treg
73 cells, we examined the Immuno-Navigator dataset to extract the genes that are most
74 correlated with Penk and with each other (Figure 2A). Among these genes, we observe
75 several members of the TNFR superfamily (*Tnfrsf1b* (TNFR2), *Tnfrsf4* (OX40), *Tnfrsf9* (4-1BB),
76 *Tnfrsf18* (GITR)) as well as the transcription factor *Batf*. Furthermore, *Batf* expression is
77 highly correlated with *Penk* in Treg (R=0.599, Figure 2B). Thus, TNFR and BATF could be
78 involved in the regulation of *Penk* in Treg. To examine this possibility, we reanalyzed our
79 previously published dataset establishing the transcriptome of Treg stimulated with anti-CD3,
80 anti-CD28 antibodies and TNFR agonists *in vitro* [18]. We observe that addition of TNFR2, OX40
81 or 4-1BB agonists increases *Penk* expression at 36h post-stimulation relative to controls
82 (Figure 2C). Interestingly, *Batf* is also increased by TNFR agonists at an earlier time point
83 (18h), suggesting that TNFR signaling may regulate *Penk* expression through the BATF
84 transcription factor. Accordingly, a dramatic decrease in *Penk* expression is observed in Treg
85 lacking BATF [19](Figure 2D). In line with our hypothesis, BATF is a crucial partner of AP-1
86 transcription factor that has been shown to regulate *Penk* in the hippocampus[20].

87 ***Penk* is prominently expressed by Treg at steady state**

88 Based on these findings, we further investigated the expression of *Penk* mRNA in various
89 immune cell types across multiple tissues, as defined by a combination of lineage markers.
90 (Figure S1A). To do so, we crossed a transgenic mouse model expressing Tamoxifen (TMX)-
91 inducible Cre recombinase under the promoter of *Penk* ($Penk^{Cre\text{-}ERT2}$) with the $ROSA26^{TdTomato}$
92 reporter mice. In these mice, any cell that would expressed *Penk* at the time of TMX
93 administration would become permanently tagged with the tdTomato reporter a few days

94 later. In order to improve detection of those cells by flow cytometry, we also used an anti-
95 mCherry that cross-react with TdTomato (Figure S1B). In lymphoid tissue, such as in lymph
96 node (LN), *Penk* expression is mainly restricted to Treg and to a small subset of activated
97 $CD4^+$ T-cells (Figure 3A). Similar results are obtained in non-lymphoid tissues, such as in the
98 colon, although *Penk* expression in activated T cells is further increased relative to LN (Figure
99 3B). As summarized in Figure 3C, Treg is the immune subset expressing the highest level of
100 *Penk* in all tissues analyzed. Expression of *Penk* is also detected in Tconv, but at lower
101 frequencies than in Treg, in agreement with the molecular meta-signature established above
102 (Figure 1). All other cell types show low or undetectable *Penk* expression. Interestingly, in
103 $CD4^+$ T-cells (Tconv and Treg), *Penk* expression is higher in the activated $CD62L^{low}$ $CD44^{high}$
104 fraction compared to the naive $CD62L^{high}$ $CD44^{low}$ phenotype (Figure S2). Thus, we observed
105 that *Penk* mRNA is predominantly found in Treg and activated $CD4^+$ T cells in the immune
106 system at steady state. Among these, the highest expression of *Penk* was detected in Treg
107 cells present in the skin and the colon. However, we cannot exclude the possibility that the
108 distribution of Penk may be broader in an inflammatory context. In line with this, a recent
109 study demonstrated that *Penk* expression in M2 macrophages is dependent on IL-4 and
110 occurs in response to nerve injury[21].

111 **Heat hyperalgesia in mice deficient for *Penk* in Treg**

112 To determine if enkephalins produced by Treg had an effect on pain at steady state, we
113 generated mice deficient for enkephalins in Treg by crossing TMX-inducible Cre recombinase
114 under the control of the *Foxp3* promoter ($Foxp3^{Cre\text{-}ERT2}$) with mice transgenic for LoxP
115 sequences flanking exon 2 of *Penk* ($Penk^{flox}$). In these mice (hereafter referred to as Lox), any

116 cell expressing Foxp3 at the time of TMX administration would become deficient for exon 2
117 of *Penk* a few days later. Since exon 2 is the precursor of Met-Enkephalin, an endogenous
118 opioid that act on thermal pain sensation[22], we evaluated the sensibility of these mice to
119 pain induced by heat (Figure 4). As controls, we used mice expressing the Cre recombinase
120 and wild-type (WT) at the locus of LoxP sequences insertion. Mice were treated with TMX
121 and evaluated for heat sensitivity without further additional treatment at ten different time
122 points (4 before and 6 after administration of TMX, 2 to 3 days apart). Under these
123 conditions, a significant trend towards lower latency periods (signing heat hyperalgesia) is
124 observed in the Lox group compared to WT mice. Interestingly, the effect is not apparent
125 until 7 days after TMX administration (Figure S4). Indeed, before TMX administration, WT and
126 Lox female and male mice do not differ in their response to heat (Figure 4A-B). However,
127 after TMX administration, Lox mice develop hyperalgesia compared to control mice, with a
128 20 percent reduction in their median latency period from D7 onwards (8.1 vs. 6.5 sec, Figure
129 4C). Interestingly, the effect of *Penk* deletion in Treg on heat hyperalgesia is sex independent,
130 since it is observed in both female and male (Figure 4D), although the reduction was slightly
131 higher in female (22% reduction in latency period) than in male (16% reduction). This can be
132 explained by the fact that males tend to respond faster (7.9s vs 6.1s) than females (8.4s vs
133 7.0s), irrespective of the genotype (Figure 4D). *Penk* expression by $CD4^+$ T-cells has been
134 associated with analgesia in mice models of visceral pain[23–25], but the specific contribution of
135 Treg was not investigated. In neuroinflammatory settings, such as constriction of the sciatic
136 nerve, pain control by Treg could be dependent on their immuno-suppressive function [12,26–28].
137 On the contrary, our tests were performed at steady state, ruling out the possibility that
138 hyperalgesia could be due to a defect in the immuno-suppressive function of Treg. They

strongly suggest a direct role of enkephalins produced by Treg on nociception, uncovering a new non-immune fundamental function of Tregs on endogenous regulation of basal somatic sensitivity.

142 **Bibliography**

143 1. Hatzioannou, A. *et al.* Regulatory T Cells in Autoimmunity and Cancer: A Duplicitous
144 Lifestyle. *Front. Immunol.* **12**, (2021).
145 2. Kim, J. M., Rasmussen, J. P. & Rudensky, A. Y. Regulatory T cells prevent catastrophic
146 autoimmunity throughout the lifespan of mice. *Nat. Immunol.* **8**, 191–197 (2007).
147 3. Nishikawa, H. & Sakaguchi, S. Regulatory T cells in tumor immunity. *Int. J. Cancer* **127**,
148 759–767 (2010).
149 4. Xiao, T. *et al.* Tregs in visceral adipose tissue up-regulate circadian-clock expression to
150 promote fitness and enforce a diurnal rhythm of lipolysis. *Sci. Immunol.* **7**, eabl7641
151 (2022).
152 5. Meng, F., Hao, P. & Du, H. Regulatory T cells differentiation in visceral adipose tissues
153 contributes to insulin resistance by regulating JAZF-1/PPAR-γ pathway. *J. Cell. Mol. Med.*
154 **27**, 553–562 (2023).
155 6. Shime, H. *et al.* Proenkephalin $^{+}$ regulatory T cells expanded by ultraviolet B exposure
156 maintain skin homeostasis with a healing function. *Proc. Natl. Acad. Sci.* **117**, 20696–
157 20705 (2020).
158 7. Dombrowski, Y. *et al.* Regulatory T cells promote myelin regeneration in the central
159 nervous system. *Nat. Neurosci.* **20**, 674–680 (2017).
160 8. Ito, M. *et al.* Brain regulatory T cells suppress astrogliosis and potentiate neurological
161 recovery. *Nature* **565**, 246–250 (2019).
162 9. Huang, Y., Liu, Z., Cao, B.-B., Qiu, Y.-H. & Peng, Y.-P. Treg Cells Attenuate
163 Neuroinflammation and Protect Neurons in a Mouse Model of Parkinson's Disease. *J.*
164 *Neuroimmune Pharmacol. Off. J. Soc. NeuroImmune Pharmacol.* **15**, 224–237 (2020).

165 10. Lemaitre, P. *et al.* Molecular and cognitive signatures of ageing partially restored through
166 synthetic delivery of IL2 to the brain. *EMBO Mol. Med.* **15**, e16805 (2023).
167 11. Austin, P. J., Kim, C. F., Perera, C. J. & Moalem-Taylor, G. Regulatory T cells attenuate
168 neuropathic pain following peripheral nerve injury and experimental autoimmune
169 neuritis. *Pain* **153**, 1916–1931 (2012).
170 12. Duffy, S. S. *et al.* Regulatory T Cells and Their Derived Cytokine, Interleukin-35, Reduce
171 Pain in Experimental Autoimmune Encephalomyelitis. *J. Neurosci. Off. J. Soc. Neurosci.*
172 **39**, 2326–2346 (2019).
173 13. Kuhn, J. A. *et al.* Regulatory T-cells inhibit microglia-induced pain hypersensitivity in
174 female mice. *eLife* **10**, e69056 (2021).
175 14. Lees, J. G., Duffy, S. S., Perera, C. J. & Moalem-Taylor, G. Depletion of Foxp3+ regulatory T
176 cells increases severity of mechanical allodynia and significantly alters systemic cytokine
177 levels following peripheral nerve injury. *Cytokine* **71**, 207–214 (2015).
178 15. Bethea, J. R. & Fischer, R. Role of Peripheral Immune Cells for Development and Recovery
179 of Chronic Pain. *Front. Immunol.* **12**, (2021).
180 16. Vandenbon, A. *et al.* Immuno-Navigator, a batch-corrected coexpression database,
181 reveals cell type-specific gene networks in the immune system. *Proc. Natl. Acad. Sci.* **113**,
182 E2393–E2402 (2016).
183 17. Zelenika, D. *et al.* Regulatory T Cells Overexpress a Subset of Th2 Gene Transcripts. *J.*
184 *Immunol.* **168**, 1069–1079 (2002).
185 18. Lubrano di Ricco, M. *et al.* Tumor necrosis factor receptor family costimulation increases
186 regulatory T-cell activation and function via NF-κB. *Eur. J. Immunol.* **50**, 972–985 (2020).

187 19. Hayatsu, N. *et al.* Analyses of a Mutant Foxp3 Allele Reveal BATF as a Critical
188 Transcription Factor in the Differentiation and Accumulation of Tissue Regulatory T Cells.
189 *Immunity* **47**, 268-283.e9 (2017).
190 20. Sonnenberg, J. L., Rauscher, F. J., Morgan, J. I. & Curran, T. Regulation of proenkephalin by
191 Fos and Jun. *Science* **246**, 1622–1625 (1989).
192 21. Celik, M. Ö., Labuz, D., Keye, J., Glauben, R. & Machelska, H. IL-4 induces M2
193 macrophages to produce sustained analgesia via opioids. *JCI Insight* **5**, (2020).
194 22. Aman, Y., Pitcher, T., Simeoli, R., Ballard, C. & Malcangio, M. Reduced thermal sensitivity
195 and increased opioidergic tone in the TASTPM mouse model of Alzheimer's disease. *PAIN*
196 **157**, 2285 (2016).
197 23. Boué, J. *et al.* Endogenous regulation of visceral pain via production of opioids by
198 colitogenic CD4(+) T cells in mice. *Gastroenterology* **146**, 166–175 (2014).
199 24. Basso, L. *et al.* Endogenous analgesia mediated by CD4(+) T lymphocytes is dependent on
200 enkephalins in mice. *J. Neuroinflammation* **13**, 132 (2016).
201 25. Basso, L. *et al.* T-lymphocyte-derived enkephalins reduce Th1/Th17 colitis and associated
202 pain in mice. *J. Gastroenterol.* **53**, 215–226 (2018).
203 26. Davoli-Ferreira, M. *et al.* Regulatory T cells counteract neuropathic pain through
204 inhibition of the Th1 response at the site of peripheral nerve injury. *Pain* **161**, 1730–1743
205 (2020).
206 27. Ledeboer, A. *et al.* Intrathecal Interleukin-10 Gene Therapy Attenuates Paclitaxel-Induced
207 Mechanical Allodynia and Proinflammatory Cytokine Expression in Dorsal Root Ganglia in
208 Rats. *Brain. Behav. Immun.* **21**, 686–698 (2007).

28. Shen, K.-F. *et al.* Interleukin-10 down-regulates voltage gated sodium channels in rat dorsal root ganglion neurons. *Exp. Neurol.* **247**, 466–475 (2013).

29. Baker, A. K., Hoffmann, V. L. H. & Meert, T. F. Dextromethorphan and ketamine potentiate the antinociceptive effects of mu- but not delta- or kappa-opioid agonists in a mouse model of acute pain. *Pharmacol. Biochem. Behav.* **74**, 73–86 (2002).

30. Shannon, P. *et al.* Cytoscape: A Software Environment for Integrated Models of Biomolecular Interaction Networks. *Genome Res.* **13**, 2498–2504 (2003).

218 **Materials & Methods**

219 **Extraction of Treg meta-signatures**

220 The datasets used were selected based on a "Treg* AND (Tconv* OR Teff*) AND Mus
221 Musculus" search in the GEO dataset web site (https://www.ncbi.nlm.nih.gov/gds). GEO
222 datasets were manually inspected for inclusion of studies comparing fresh Treg with fresh
223 Tconv from lymphoid organs. Characteristics of selected datasets are summarized in Table 1.
224 For each dataset, we generated a list of differentially expressed genes with a cutoff based on
225 a false discovery rate (FDR) inferior to 0.05 and a log2 fold change superior to 1 with the
226 GEO2R embedded algorithm.

227 **Table 1: Characteristics of the datasets used for the Treg meta-signature** (NA = not
228 available; LN = Lymph Nodes)

Dataset	Genetic background	Age	Sex	Treg sorting	Tissue	Affymetrix Genome array
GSE103216	C57Bl/6	6-8 weeks	Female	Foxp3-RFP	LN	1.0
GSE136582	C57Bl/6	6-8 weeks	NA	Foxp3-eGFP	Spleen	2.0
GSE14308	C57Bl/6	NA	NA	$CD25^{high}$	Spleen and LN	2.0
GSE15907	C57Bl/6	6 weeks	Male	$CD25^{high}$	Spleen	1.0
GSE17580	C57Bl/6	NA	Female	$CD25^{high}$	Mesenteric LN	2.0
GSE24210	C57Bl/6	NA	NA	$CD25^{high}$	Spleen and LN	2.0
GSE37532	C57Bl/6	25 weeks	Male	$CD25^{high}$	LN	1.0
GSE40685	C57Bl/6	NA	NA	Foxp3-GFP	Spleen and LN	2.0
GSE42021	BALB/c	NA	NA	Foxp3-GFP	Spleen and LN	2.0
GSE50096	C57Bl/6	6 weeks	NA	Foxp3-GFP	Spleen	1.0
GSE7460	C57Bl/6	32-36 weeks	NA	$CD25^{high}$	LN	2.0

229

230 **Mice**

231 All male and female mice were on a C57Bl/6J background. *Foxp3*$^{tm9(EGFP/cre/ERT2)Ayr}$/J (Foxp3$^{Cre\text{-}ERT2}$)
232 (catalog #016961), *B6.Cg-Gt(ROSA)26Sor*$^{tm9(CAG\text{-}tdTomato)Hze}$*/J* (ROSA ^{tdTomato}) (catalog #007909),
233 *B6.Cg-Penk*$^{tm1.1(cre/ERT2)Hze}$*/J,* (Penk$^{Cre\text{-}ERT2}$) (catalog #022862) were purchased from The Jackson
234 Laboratory. *C57BL/6JSmoc-Penk*$^{em1(flox)Smoc}$ (Penk^{flox}) were purchased from Shanghai Model
235 Organisms (catalog NM-CKO-210032). For the *Penk* mapping experiments, Penk$^{Cre\text{-}ERT2}$ were
236 bred with ROSA^{tdtomato}. All mice were confirmed to be homozygous for the inducible Cre and
237 at least heterozygous for tdTomato by touchdown PCR (primers sequences available on
238 request). To specifically knock-out the Penk gene in Tregs, Foxp3$^{Cre\text{-}ERT2}$ were crossed with
239 Penk^{flox} leading to double heterozygous mice (F1) that were crossed together resulting in
240 double homozygous F2 littermates' mice. All mice used in this study were of F3 generation.
241 Mice were genotyped by touchdown PCR (primers sequences available on request). Mice
242 were housed under specific pathogen-free conditions and were used for experiments at 8
243 weeks or older. All protocols were approved by the Ethics Committee for Animal
244 Experimentation Charles Darwin (APAFIS #32284-2021070513305185 v5).

245 **Tamoxifen administration**

246 Tamoxifen (ThermoFisher, Les Ulis, France) was dissolved in peanut oil at the concentration
247 of 8 mg/ml under 37°C agitation and delivered by 200µL oral gavage. All mice were
248 administered tamoxifen only once, 7 days before the start of each experiment.

249 **Preparation of cell suspensions**

250 Organs were harvested on ice in PBS 3% fetal calf serum (FCS). Inguinal, brachial and
251 mesenteric LNs and spleens were directly mashed through a 70µm filter and resuspended in

252 PBS 3% FCS. Lungs, colons, livers, VAT and skin were dissected, minced then incubated in
253 appropriate digestion buffers (Miltenyi Biotech, Paris, France) at 37°C for various duration
254 according to manufacturer protocols. Cell suspensions were then passed through a 70µm cell
255 strainer and suspended in PBS 3% FCS. To eliminate dead cells and debris, liver cell
256 suspensions was isolated on a 70:30 Percoll gradient. Rings were collected, washed, and cell
257 pellets were resuspended in PBS 3% FCS. ACK Lysing Buffer was used to lyse red blood cells in
258 the lungs, livers and spleens (lysis performed for 1 min at RT, followed by two washes with
259 PBS), prior to staining for flow cytometry.

260 **Antibodies and flow cytometry analysis**

261 The monoclonal antibodies (mAb) and fluorescent reagents used in this study are listed
262 below in the Table. Up to 4.10^6 cells were incubated for 30 min at 4°C with fixable live/dead
263 dye and with the anti-CD16/CD32 (clone 2.4G2) to block FcgRII and FcgRII receptors. Cells
264 were then stained with a combination of antibodies. Cell-surface staining was performed in
265 PBS 3% FCS for 20 min at 4°C. Permeabilization and intracellular staining was performed
266 using the Foxp3/Transcription Factor Staining Buffer Set kit and protocol (ThermoFisher).
267 Stained cells were washed with PBS 1X before acquisition on a Cytek Aurora flow cytometer
268 (Cytek Bioscience, Fremont, CA, USA). Data were analyzed and UMAPs were generated using
269 FlowJo software, version 10.8.1 (TreeStar, Ashland, OR, USA).

mAb or reagent (dye)	Provider	Clone	Dilution
Anti-mouse F4/80 (AF647)	BioLegend	BM8	1/400
Anti-mouse CD62L (AF700)	BD Biosciences	MEL-14	1/400
Anti-mouse CD25 (APC Fire 750)	Biolegend	PC61	1/100

Anti-mouse CD4 (BUV 496)	Miltenyi Biotec	GK1.5	1/400
Anti-mouse CD3 (BUV563)	BD Biosciences	145-2C11	1/400
Anti-mouse CD69 (BUV661)	BD Biosciences	H1.2F3	1/200
Anti-mouse Nkp46 (BUV737)	BD Biosciences	29A1.4	1/200
Anti-mouse CD8a (BUV805)	BD Biosciences	53-6.7	1/800
Anti-mouse Ly6G (BV570)	BioLegend	1A8	1/200
Anti-mouse CD11b (BV650)	BD Biosciences	M1/70	1/1000
Anti-mouse CD45 (NovaFluor Blue 660-120S)	eBioscience	30-F11	1/200
Anti-mouse CD11c (PE CF594)	BD Biosciences	HL3	1/150
Anti-mouse Ly6C (PE Cy7)	BD Biosciences	AL-21	1/1600
Anti-mouse CD44 (PerCP)	BioLegend	IM7	1/200
Anti-mouse CD19 (PerCP Cy5.5)	BD Biosciences	1D3	1/400
Anti-mouse IA/IE (V500)	BD Biosciences	M5/114.15.2	1/300
Anti-mouse TCRγδ (BV421)	eBioscience	GL3	1/200
Anti-mouse Ki67 (AF532)	Invitrogen/eBiosience	SolA15	1/1600
Anti-mouse mCherry (Pacific Blue)	Invitrogen/eBiosience	16D7	1/50
Anti-mouse GATA3 (PE Cy5)	Invitrogen/eBioscience	TWAJ	1/400
Anti-mouse Foxp3 (FITC)	Invitrogen/eBioscience	FJK-16s	1/800
Fixable viability dye (Live Dead Blue)	Invitrogen/eBioscience		1/2000
Anti-mouse CD16/CD32 (BD Fc Block)	BD Biosciences	2.4G2	1/80

Hot plate test

The method used was described by Baker et al. (2002)[29]. Briefly, mice were placed on a metal hot plate maintained at 55°C. The plate was enclosed with Plexiglas walls so that mice could not escape. The response latency, which is the time taken to observe a nocifensive behavior

275 such as jumping, licking or flicking of the hind paws, was recorded. The mice were then
276 immediately removed from the plate upon the recording of a reaction, or within 25s if no
277 response was observed to prevent tissue damage. The test was repeated every two days for
278 a total of four measures before the administration of tamoxifen and four measures starting
279 from D3 post-tamoxifen. Male and female mice were tested separately. Mice remained in
280 their home cage except when being tested on the hot plate. The experimenter was blind to
281 the genotype of the mice until the end of the experiment.

282 **Statistical analysis**

283 All statistical tests are reported in the figure legends and were performed with Prism v8
284 (Graph Pad Inc, La Jolla, CA, USA). The statistical power of the analyses (alpha) was set at
285 0.05.

286 **Funding**

287 This study was funded by a research grant from Sorbonne University (SU) (Emergence 2021)
288 to GM, and by the National Institute for Health and Medical Research (INSERM). NA was
289 funded by a doctoral fellowship from Fondation ARC and by a post-doctoral fellowhip from
290 EGLE TX, MF by a doctoral fellowship from the French Ministère de l'Enseignement Supérieur
291 et de la Recherche, MP and MN by pregraduates fellowships from SU and EGLE TX
292 respectively. The funders had no role on the supervision of the research, nor in the analysis
293 of the results.

294 **Acknowledgments**

The authors would like to thank Olivier Brégerie, Flora Issert, and Doriane Foret for taking care of our mice; Dr Martina Lubrano di Ricco and Morgane Hilaire for technical help, Dr Benoit Salomon for providing Foxp3$^{Cre\text{-}ERT2}$ and ROSA^{tdTomato} mice; Francois-Xavier Lejeune (ICM, Paris) for help with biostatistics analysis and Dr Jean-Luc Teillaud for critical review of the manuscript.

301 **Figure 1: A meta signature of murine Treg and *Penk* mRNA expression in lymphoid and non**
302 **lymphoid organs. A)** Top 25 genes enriched in Treg compared to Tconv from lymphoid tissue
303 from at least 10 of the 11 datasets analyzed ranked by fold change (LogFC) of mean
304 expression relative to Tconv. The *Penk* gene is highlighted in red. **B)** Correlation of Penk and
305 Foxp3 mRNA expression in all the cell types listed in the legend. The Pearson correlation
306 coefficient is indicated. **C)** Expression of Penk mRNA in Treg (blue) and Tconv (red) isolated
307 from thymus, visceral adipose tissue (VAT) and muscle. The source of the data is indicated
308 below each graph.

309

310 **Figure 2: Penk mRNA expression is regulated by TNFR signaling and the BATF transcription**
311 **factor in Treg. A)** A network of the genes most correlated to Penk in Treg is shown. The
312 Pearson correlation values were extracted from the Immuno-Navigator database (taking only
313 Treg for the analysis) and integrated into Cytoscape v3.7[30]. Each node is a gene linked by
314 edges with width proportional to the Pearson correlation. (edge range: 0.538-0.758). **B)**
315 Illustration of the correlation between expression of *Penk* and *Batf* in Treg. Each dot is a
316 sample from the Immuno-Navigator database. The Pearson correlation coefficient is
317 indicated on the figure. **C)** *Penk* and *Batf* mRNA expression after *in vitro* stimulation of
318 purified Treg with the indicated TNFR agonists prior (0), and at 18 and 36hrs after
319 stimulation. Each dot is a biological replicate from a single experiment. **D)** GEO2R analysis of
320 the GSE89656 dataset for Penk mRNA variations between wild type control Treg (WT) and
321 BATF-KO Treg.

322

323 **Figure 3: *Penk* is prominently expressed by Treg at steady state**

324 **A-B)** (right) UMAP representing all major cell types indicated in the figures determined by
325 flow cytometry from lymph nodes (A) and colon (B) (left). Projection of *Penk* (blue) on the
326 UMAP of lymph node and colon (right). Subsets were manually gated as depicted in Figure
327 S1A. **C)** Scatter plot displaying the average population size and percentage of $Penk^+$ cells for
328 the listed cell populations and organs. Population size was calculated as the percentage out
329 of total $CD45^+$ single cells and represented on a log10 scale. (n = 3 mice for the VAT, spleen
330 and bone marrow, n = 6 mice for the other groups; results cumulative of two independent
331 experiments).

332

333 **Figure 4: Heat hyperalgesia in mice deficient for *Penk* in Treg. A)** Withdrawal latency of WT
334 and Lox mice before the administration of TMX (baseline). The mean of all 4 measures before
335 administration of TMX for each mouse is shown. Statistical modeling was performed using a
336 non parametric unpaired Mann-Whitney t-test and was deemed as non-significant (ns). **B)**
337 Withdrawal latency of WT and Lox mice before administration of TMX (baseline) shown
338 separately for female and male mice, as in A. Statistical modeling was performed using two-
339 way ANOVA and the effect of the genotype on the results was deemed non-significant (ns).
340 **C)** Withdrawal latency of WT and Lox mice post-TMX treatment. The mean of all 4 measures
341 taken from D7 onward is represented for each mouse. Statistical modeling was performed
342 using a non parametric unpaired Mann-Whitney t-test and was deemed significant
343 (p=0,0038). **D)** Withdrawal latency of WT and Lox mice post-TMX treatment shown
344 separately for female and male mice, as in C. Statistical modeling was performed using two-

345 way ANOVA and the effect of the genotype on the results was deemed significant (p=0,0037).
346 A multiple comparisons test using the Benjamini-Hochberg False Discovery Rate model was
347 used. The adjusted p values were deemed significant for both female and male mice
348 (q=0,043). Results shown in this figure are cumulative of two independent experiments with
349 n = 44 mice (26 WT and 18 Lox).

350 **Supplementary figures and table**

351 **Figure S1. Representative flow cytometry profiles in Penk$^{Cre\text{-}ERT2}$x ROSA^{tdtomato}**

352 **A)** Gating strategy used to define the population for the mapping of *Penk* expression by
353 immune cells. **B)** Representative staining of TdTomato and mCherry

354

355 **Figure S2. *Penk* expression in Tconv and Treg according to activation status in lymph node**

356 Representative staining of TdTomato and mCherry in naive (CD62L^{high} CD44^{low}), central
357 memory (CD62L^{high} CD44^{high}) and effector memory (CD62L^{low} CD44^{high}) Tconv (top) and Treg
358 (bottom).

359

360 **Figure S3. A kinetics of latency periods in response to heat in WT and Lox mice.** Each dot is
361 the mean value (± SD) of latency period in response to heat stimulation for all mice of the WT
362 or Lox genotype. The results are represented as a function of days relative to TMX gavage
363 (D0). Statistical modeling of the results was performed with linear regression curve fitting
364 with a comparison of intercept and slopes. The low p value allow to reject the hypothesis
365 that one curve fits all the datasets.

366

367 **Table S1: List of the differentially expressed genes between Tconv and Treg.** Only genes
368 upregulated in 10 out of 11 datasets are presented with the associated log2 fold change as
369 determined by GEO2R. (NA = not available)

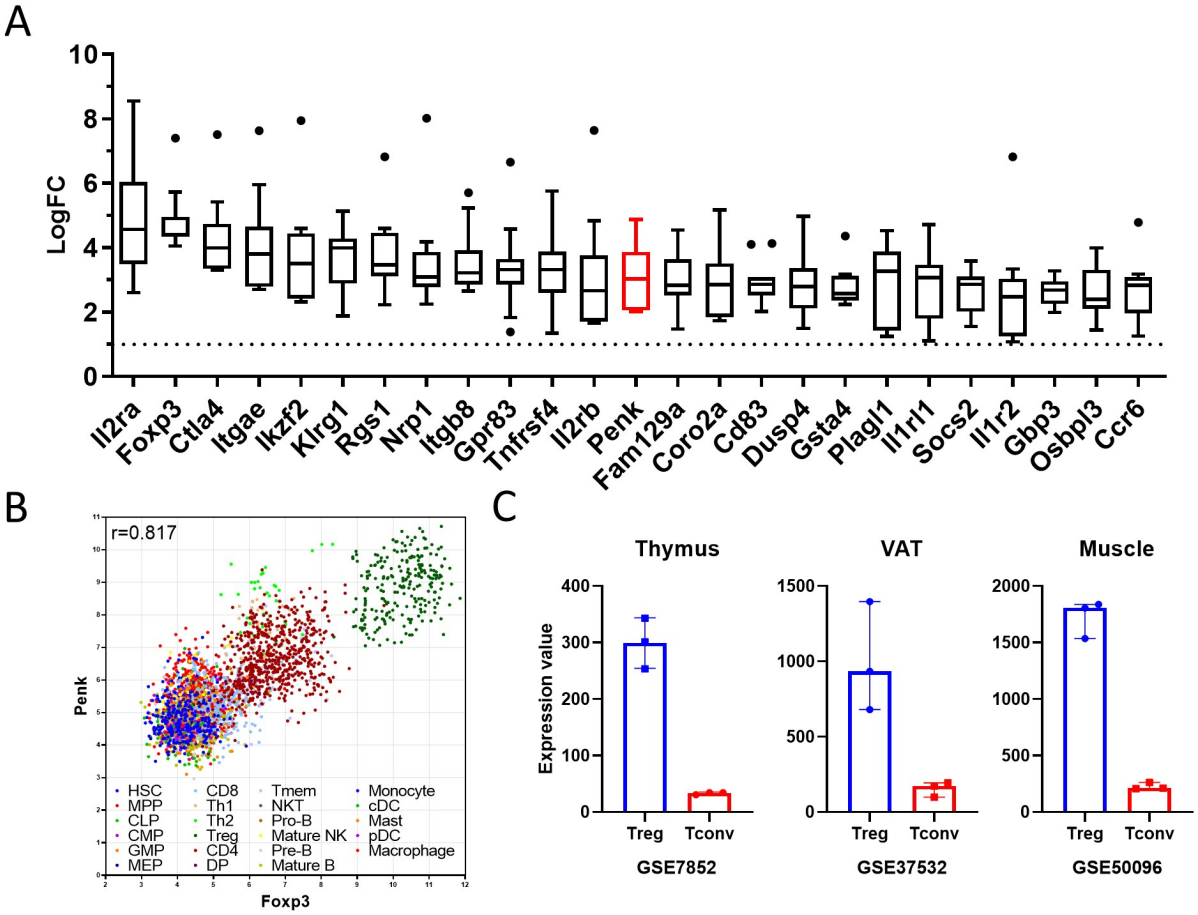
A
LogFC
10
8
6
4
2
0
Il2ra
Foxp3
Ctla4
Itgae
Ikzf2
Klrg1
Rgs1
Nrp1
Itgb8
Gpr83
Tnfrsf4
Il2rb
Penk
Fam129a
Coro2a
Cd83
Dusp4
Gsta4
Plagl1
Il1rl1
Socs2
Il1r2
Gbp3
Osbpl3
Ccr6
B
r=0.817
Penk
Foxp3
HSC
MPP
CLP
CMP
GMP
MEP
CD8
Th1
Th2
Treg
CD4
DP
Tmem
NKT
Pro-B
Mature NK
Pre-B
Mature B
Monocyte
cDC
Mast
pDC
Macrophage
C
Thymus
VAT
Muscle
Expression value
Treg
Tconv
GSE7852
GSE37532
GSE50096

Figure 1

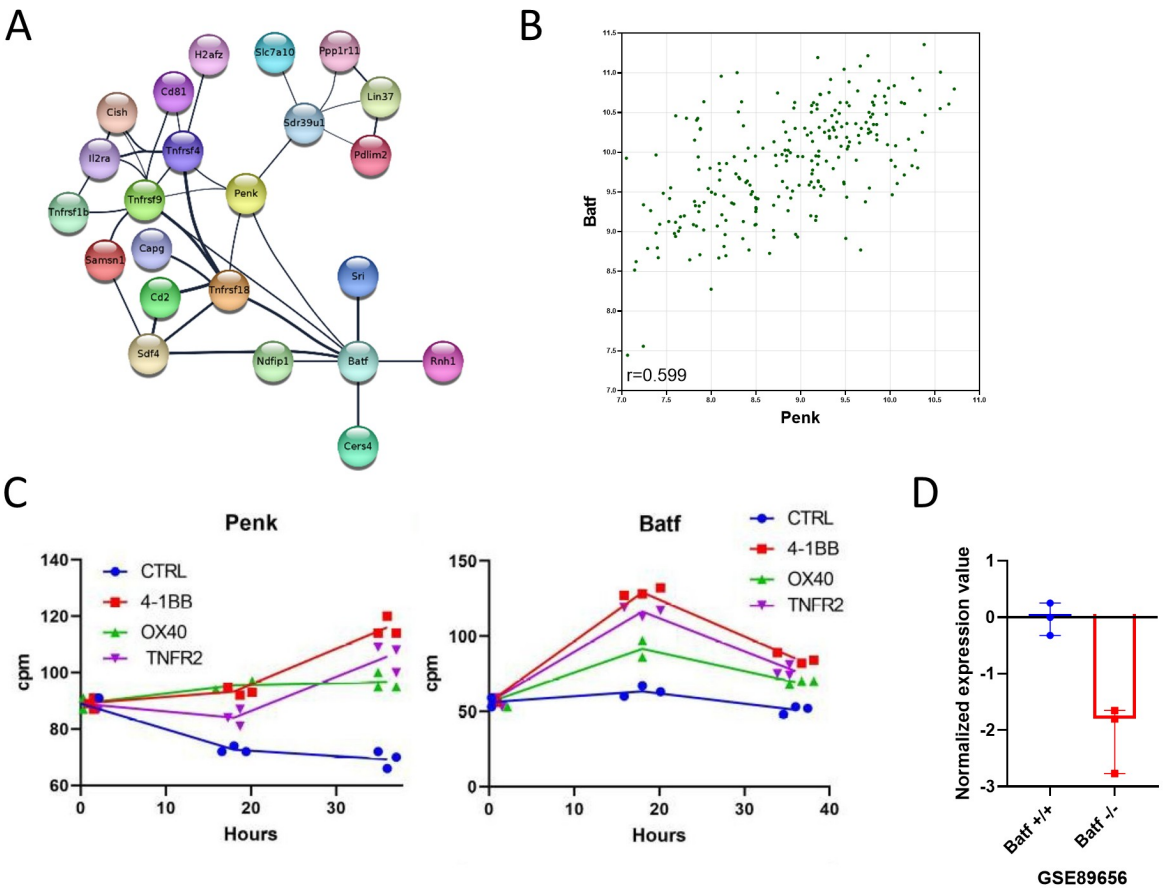
A
H2afz
Slc7a10
Ppp1r11
Cd81
Lin37
Cish
Sdr39u1
Il2ra
Tnfrsf4
Pdlim2
Tnfrsf1b
Tnfrsf9
Penk
Capg
Samsn1
Sri
Cd2
Tnfrsf18
Sdf4
Ndfip1
Batf
Rnh1
Cers4
B
Batf
Penk
r=0.599
C
Penk
CTRL
4-1BB
OX40
TNFR2
cpm
Hours
Batf
D
Normalized expression value
Batf +/+
Batf -/-
GSE89656

Figure 2

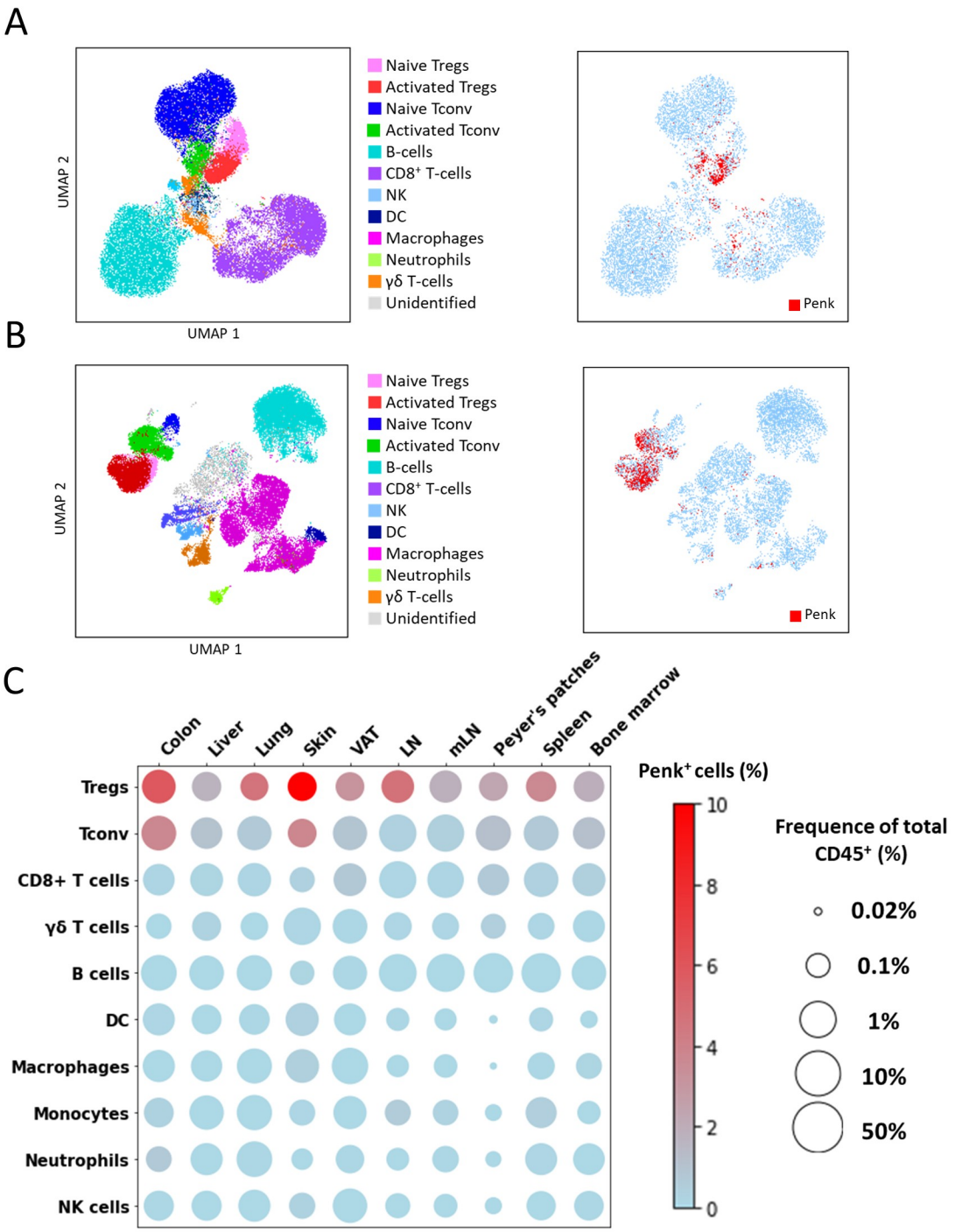
A
UMAP 2
UMAP 1
Naive Tregs
Activated Tregs
Naive Tconv
Activated Tconv
B-cells
CD8⁺ T-cells
NK
DC
Macrophages
Neutrophils
γδ T-cells
Unidentified
Penk
B
UMAP 2
UMAP 1
Naive Tregs
Activated Tregs
Naive Tconv
Activated Tconv
B-cells
CD8⁺ T-cells
NK
DC
Macrophages
Neutrophils
γδ T-cells
Unidentified
Penk
C
Colon
Liver
Lung
Skin
VAT
LN
mLN
Peyer's patches
Spleen
Bone marrow
Tregs
Tconv
CD8+ T cells
γδ T cells
B cells
DC
Macrophages
Monocytes
Neutrophils
NK cells
Penk⁺ cells (%)
10
8
6
4
2
0
Frequence of total CD45⁺ (%)
0.02%
0.1%
1%
10%
50%

Figure 3

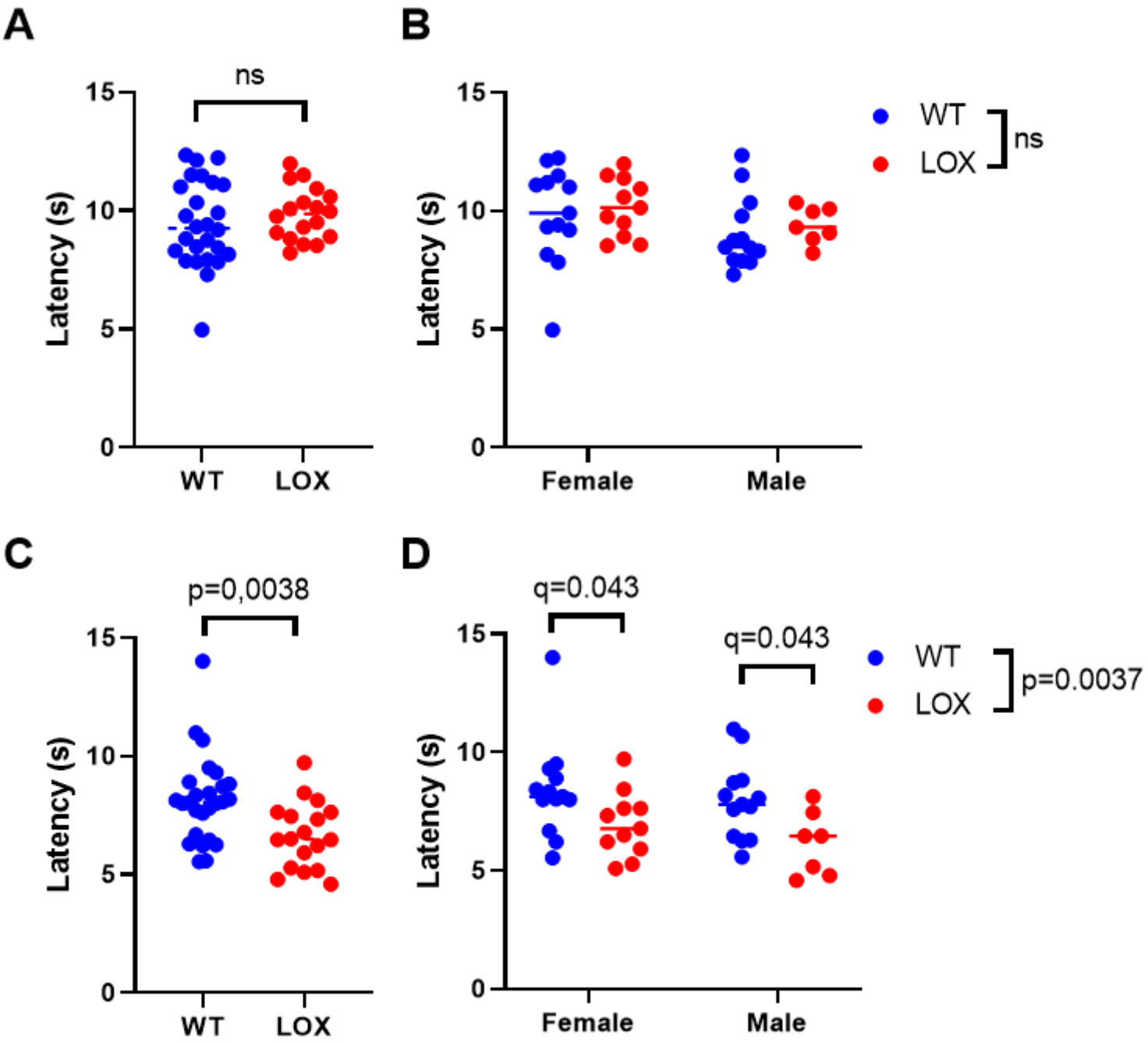
A
ns
15
10
5
0
Latency (s)
WT
LOX
B
15
10
5
0
Latency (s)
Female
Male
WT
LOX
ns
C
p=0,0038
15
10
5
0
Latency (s)
WT
LOX
D
q=0.043
q=0.043
15
10
5
0
Latency (s)
Female
Male
WT
LOX
p=0.0037

Figure 4

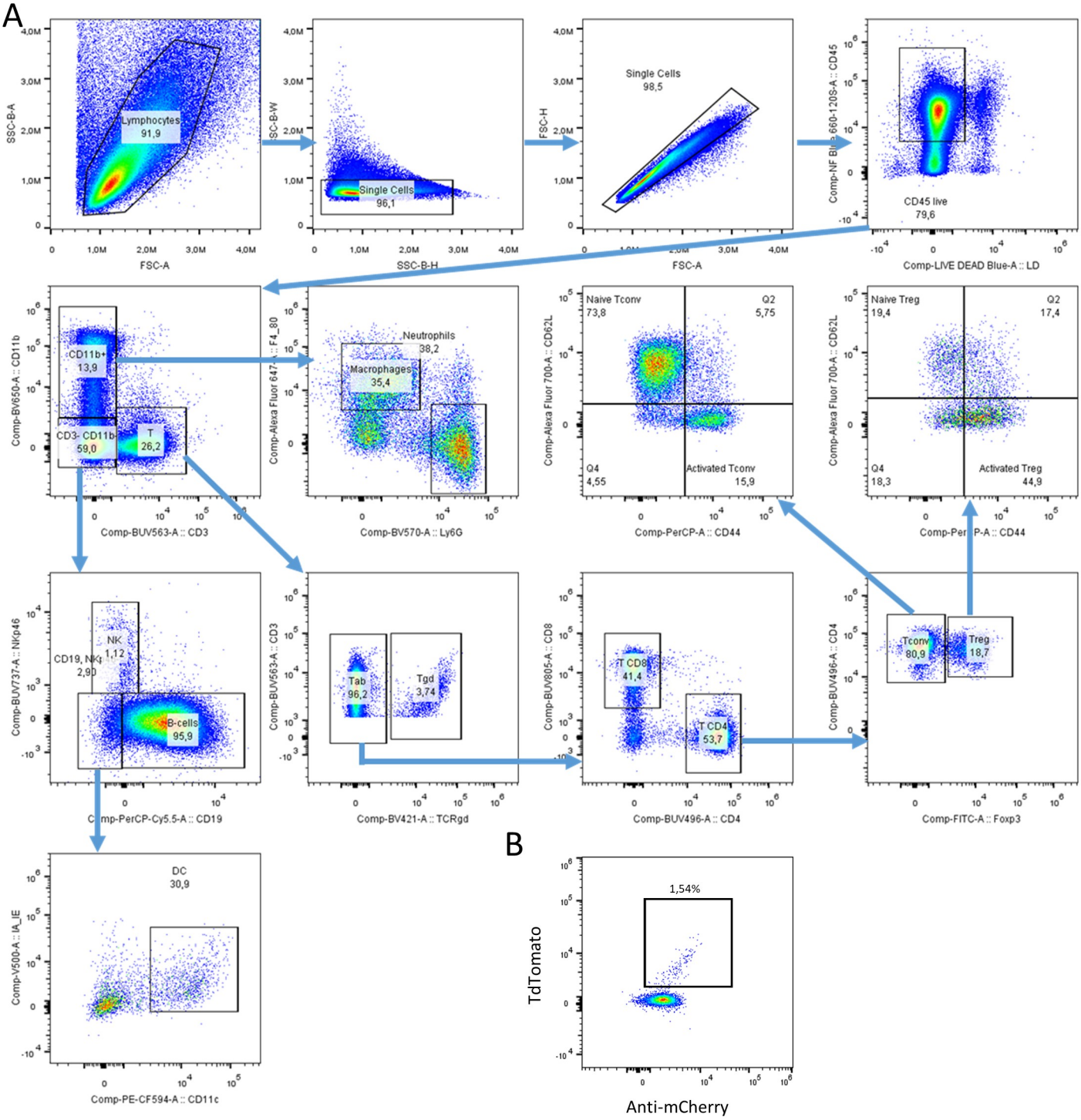
A
Lymphocytes
91,9
SSC-B-A
FSC-A
Single Cells
96,1
SSC-B-W
SSC-B-H
Single Cells
98,5
FSC-H
FSC-A
CD45 live
79,6
Comp-LIVE DEAD Blue-A :: LD
CD11b+
13,9
CD3- CD11b-
59,0
T
26,2
Comp-BV650-A :: CD11b
Comp-BUV563-A :: CD3
Neutrophils
38,2
Macrophages
35,4
Comp-BV570-A :: Ly6G
Naive Tconv
73,8
Q2
5,75
Q4
4,55
Activated Tconv
15,9
Comp-PerCP-A :: CD44
Naive Treg
19,4
Q2
17,4
Q4
18,3
Activated Treg
44,9
NK
1,12
CD19, NKp
2,90
B-cells
95,9
Comp-BUV737-A :: NKp46
Tab
96,2
Tgd
3,74
Comp-BV421-A :: TCRgd
T CD8
41,4
T CD4
53,7
Comp-BUV496-A :: CD4
Tconv
80,9
Treg
18,7
Comp-FITC-A :: Foxp3
DC
30,9
Comp-V500-A :: IA_IE
Comp-PE-CF594-A :: CD11c
B
1,54%
TdTomato
Anti-mCherry

Figure S1

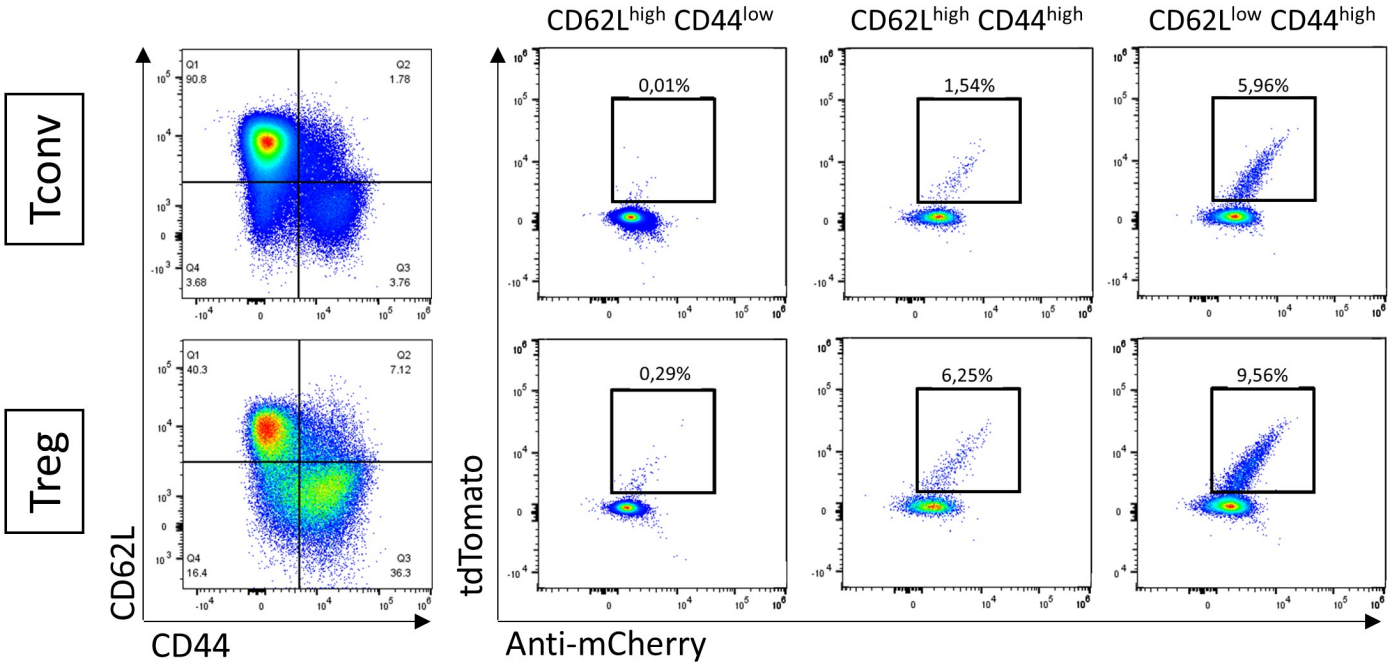
Tconv
Treg
CD62L
CD44
Q1
90.8
Q2
1.78
Q4
3.68
Q3
3.76
Q1
40.3
Q2
7.12
Q4
16.4
Q3
36.3
CD62L^high CD44^low
CD62L^high CD44^high
CD62L^low CD44^high
tdTomato
Anti-mCherry
0,01%
1,54%
5,96%
0,29%
6,25%
9,56%

Figure S2

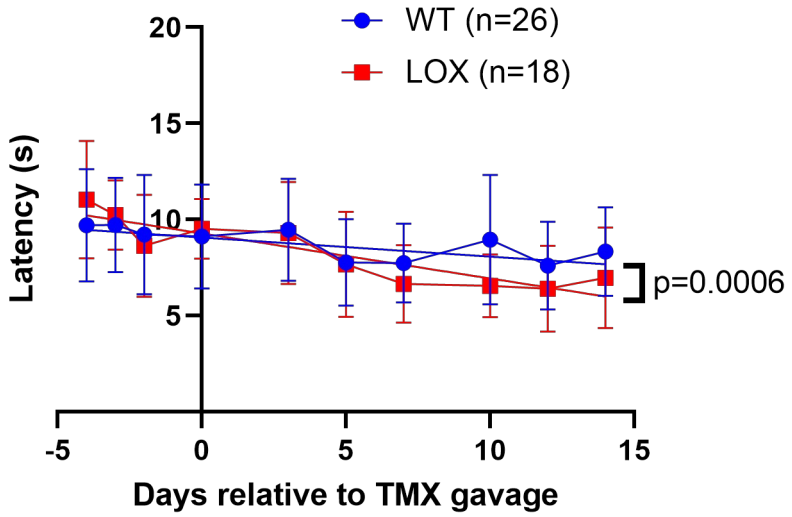
WT (n=26)
LOX (n=18)
Latency (s)
20
15
10
5
p=0.0006
-5
0
5
10
15
Days relative to TMX gavage

Figure S3